Published in final edited form as:

Cell Rep. 2021 August 03; 36(5): 109467. doi:10.1016/j.celrep.2021.109467.

A subthreshold synaptic mechanism regulating BDNF expression and resting synaptic strength

Patricia M. Horvath[1,2], **Natali L. Chanaday**[1], **Baris Alten**[1,3], **Ege T. Kavalali**[1,3,4], **Lisa M. Monteggia**[1,3,4,5,*]

[1]Department of Pharmacology, Vanderbilt University, Nashville, TN 37235, USA

[2]Department of Neuroscience, the University of Texas Southwestern Medical Center, Dallas, TX 75390, USA

[3]Vanderbilt Brain Institute, Vanderbilt University, Nashville, TN 37235, USA

[4]Senior author

[5]Lead contact

SUMMARY

Recent studies have demonstrated that protein translation can be regulated by spontaneous excitatory neurotransmission. However, the impact of spontaneous neurotransmitter release on gene transcription remains unclear. Here, we study the effects of the balance between inhibitory and excitatory spontaneous neurotransmission on brain-derived neurotrophic factor (BDNF) regulation and synaptic plasticity. Blockade of spontaneous inhibitory events leads to an increase in the transcription of *Bdnf* and *Npas4* through altered synaptic calcium signaling, which can be blocked by antagonism of NMDA receptors (NMDARs) or L-type voltage-gated calcium channels (VGCCs). Transcription is bidirectionally altered by manipulating spontaneous inhibitory, but not excitatory, currents. Moreover, blocking spontaneous inhibitory events leads to multiplicative downscaling of excitatory synaptic strength in a manner that is dependent on both transcription and BDNF signaling. These results reveal a role for spontaneous inhibitory neurotransmission in BDNF signaling that sets excitatory synaptic strength at rest.

In brief

*Correspondence: lisa.monteggia@vanderbilt.edu.

AUTHOR CONTRIBUTIONS

Conceptualization, P.M.H., E.T.K., and L.M.M.; Methodology, P.M.H., E.T.K., and N.L.C.; Investigation, P.M.H., N.L.C., and B.A.; Writing – Original Draft, P.M.H., N.L.C., E.T.K., and L.M.M.; Writing – Review & Editing, P.M.H., N.L.C., B.A., E.T.K., and L.M.M.; Supervision, E.T.K. and L.M.M.; Funding Acquisition, B.A., E.T.K., and L.M.M.

SUPPLEMENTAL INFORMATION

Supplemental information can be found online at https://doi.org/10.1016/j.celrep.2021.109467.

DECLARATION OF INTERESTS

The authors declare no competing interests.

INCLUSION AND DIVERSITY

We worked to ensure sex balance in the selection of non-human subjects. One or more of the authors of this paper self-identifies as a member of the LGBTQ+ community.

Horvath et al. study spontaneous neurotransmission to demonstrate a primary role for inhibition in gene transcription and synaptic plasticity. Inhibitory current through $GABA_A$Rs, but not excitatory current through AMPARs, bi-directionally regulates transcription of *Bdnf* and *Npas4* at rest. Control over transcription of *Bdnf* enables mIPSC-driven regulation of excitatory synaptic weight.

Graphical abstract

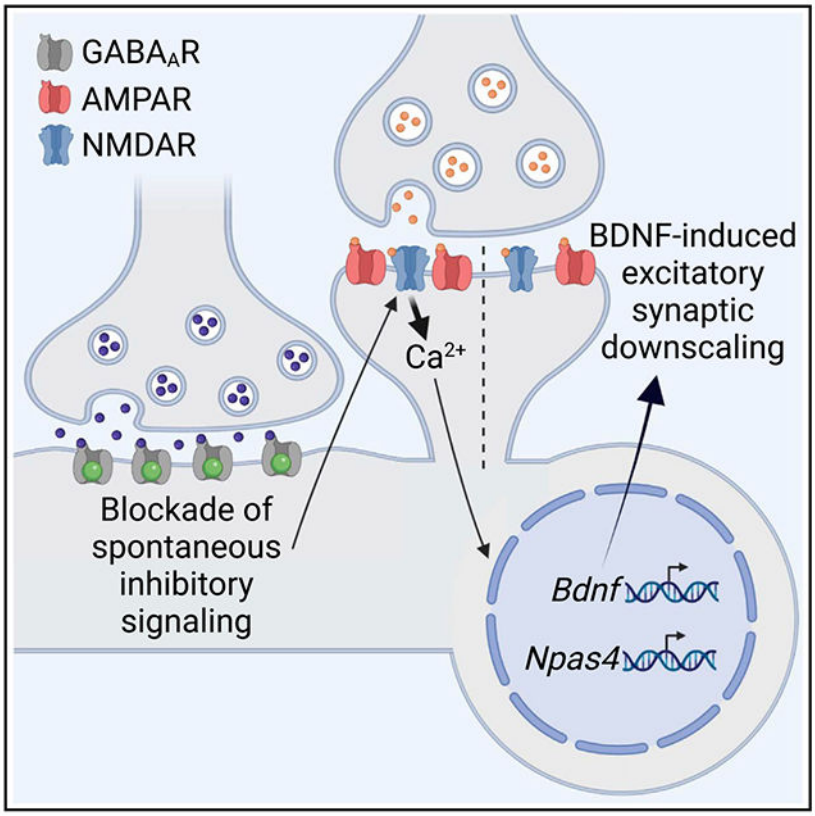

INTRODUCTION

Brain-derived neurotrophic factor (BDNF) is a critical regulator of synaptic strength and plasticity and is implicated as a key molecule in the pathophysiology and treatment of neuropsychiatric disorders (Duman and Monteggia, 2006; Autry and Monteggia, 2012). Previous studies have demonstrated that application of exogenous BDNF can increase or decrease synaptic strength depending on the duration of application (Rutherford et al., 1998; Reimers et al., 2014; Corrêa et al., 2012). Similarly, increasing endogenous local translation and release of BDNF through blockade of spontaneous excitatory neurotransmission triggers synaptic scaling to augment synaptic strength (Nosyreva et al., 2013; Autry et al., 2011). These findings suggest endogenous BDNF regulation is finely tuned by excitatory neurotransmission, such that even spontaneous neurotransmission—an action potential-independent, highly regulated form of neurotransmitter release (Kavalali, 2015)—can regulate BDNF and alter synaptic strength. Given that BDNF is involved in neuropsychiatric disorders, which are characterized by both aberrant excitatory and

inhibitory neurotransmission (Rubenstein and Merzenich, 2003; Kalueff and Nutt, 2007; Duman et al., 2019; Dienel and Lewis, 2019; Marín, 2012), we hypothesized that BDNF may also be regulated by inhibition. Although studies to date have focused on excitation and the induction of BDNF expression following depolarization as an activity-induced gene, whether BDNF can be directly regulated by inhibition to alter synaptic strength is an open question (Tao et al., 1998; Flavell and Greenberg, 2008; Park and Poo, 2013). Here, we aimed to explore the effects of spontaneous inhibitory transmission on transcription and translation of BDNF, as well as on BDNF-mediated effects on synaptic physiology.

RESULTS

Spontaneous mIPSCs regulate transcription of *Bdnf* and *Npas4*

To test for a role of inhibitory neurotransmission in regulating BDNF, we measured *Bdnf* mRNA expression and its transcription factor *Npas4* in hippocampal cultures following blockade of inhibition with picrotoxin (PTX), a use-dependent γ-aminobutyric acid A receptor ($GABA_AR$) antagonist (Figure 1A). Blocking inhibitory input in the presence of neuronal activity led to an increase in *Bdnf* and *Npas4* mRNA (Figures 1B and 1E), as expected due to increased excitatory network activity. Spontaneous neurotransmission may also elicit signaling to the nucleus, as suggested by earlier studies of the transcriptional response to inactivity (Li et al., 2020; Schaukowitch et al., 2017). Therefore, to circumvent confounding increases in network activity we used tetrodotoxin (TTX) to block action potential-mediated activity, leaving only spontaneous neurotransmission intact. Blocking inhibitory input in the absence of neuronal activity also led to an increase in *Bdnf* and *Npas4* mRNA, albeit to a smaller degree (Figures 1C and 1F), suggesting that blocking only miniature inhibitory postsynaptic currents (mIPSCs) in the absence of activity is sufficient to increase transcription. This effect is specific because blocking mIPSCs did not significantly increase the expression of two other activity-induced genes—*Cfos* and *Arc* (Figures S1A and S1B). Blocking mIPSCs with bicuculline also increased *Bdnf* and *Npas4* mRNA; the effect was not due to an off target effect of PTX (Figures 1C, 1D, 1F, and 1G).

The specificity of our qPCR data led us to examine whether mIPSCs regulate the same or a different gene set as inhibition in the presence of activity. To answer this question, we performed RNA sequencing (RNA-seq, SRA: PRJNA734956) on hippocampal neurons at baseline and following 6 h of PTX, TTX, or TTX/PTX treatment. As expected, blockade of $GABA_ARs$ with PTX in the presence of activity led to increased expression of many activity-dependent genes (Figure 1H; Table S2). Surprisingly, blocking mIPSCs increased expression of ten genes, all of which were also upregulated by blocking inhibition in the presence of activity (Figures 1I and S1C; Table S3). These data reveal the precise targeting of specific genes by mIPSCs, because the identified genes do not simply represent the most induced genes from the activity-dependent set. Of note, *Bdnf* and its transcription factor *Npas4* were included in the identified upregulated genes following mIPSC block, confirming them as key molecules regulated by inhibition.

In an effort to understand the upstream molecular regulators of *Bdnf*, we examined *Bdnf* and *Npas4* mRNA levels following 30 min of mIPSC block. *Bdnf* levels are unaltered after 30 min; however, in line with its role as a transcription factor for *Bdnf* and early response

gene, *Npas4* mRNA levels trended toward an increase (Figures S1D and S1E). Because *Bdnf* and *Npas4* are regulated by both mIPSCs and network activity, we tested the involvement of two classic intermediate molecules involved in activity-dependent transcription, ERK and CREB, in mIPSC signaling to the nucleus (Bito et al., 1996; Flavell and Greenberg, 2008; Tyssowski et al., 2018; Thomas and Huganir, 2004; Obrietan et al., 2002; Tao et al., 1998; Funahashi et al., 2019) (Figure S1F). Although blocking inhibitory input for 30 min in the presence of activity led to an increase in phosphorylation of ERK and CREB as expected, no such increase was seen upon 30 min of mIPSC blockade, indicating that mIPSCs may signal in a different manner than evoked activity (Figures S1G and S1H). However, we cannot exclude the possibility of subtle cell-type-specific or compartment-specific changes in ERK and CREB phosphorylation.

Neurons sense altered inhibitory current at rest

Blocking inhibitory input in the presence of activity leads to disinhibition of excitation that is understood to be the direct cause of increased transcription of activity-induced genes such as *Bdnf* and *Npas4*. Therefore, we examined whether an increase in excitatory signaling following mIPSC blockade was responsible for increased *Bdnf* and *Npas4* expression. We utilized whole-cell patch current clamp to simultaneously measure spontaneous depolarizing and hyperpolarizing membrane potential changes in the presence of TTX (Figures 2A and S2A) and then examined the effect of blocking miniature inhibitory postsynaptic potentials (mIPSPs). Blockade of mIPSPs for 8 min had no effect on membrane input resistance as measured at the soma (Figures 2B and 2C) and led to a modest, but significant, hyperpolarization in membrane potential (Figure 2D). Moreover, miniature excitatory postsynaptic potentials (mEPSPs) were unaffected by blockade of mIPSPs (Figures S2A–S2D). Together, these data suggest that blocking inhibitory spontaneous input in the absence of activity does not push the neuron toward an excited state.

This result led us to consider two distinct possibilities. Neurons may either adjust transcription according to the excitation/inhibition (E/I) current balance or to levels of inhibition alone at rest. If the former is true, we would expect an increase in *Bdnf* and *Npas4* expression following increased excitation at rest. To test this premise, we utilized CX614, a positive allosteric modulator of α-amino-3-hydroxy-5-methyl-4-isoxazolepropionic acid receptors (AMPARs) (Figures 2E–2J) (Arai et al., 2000). Importantly, CX614 does not affect mIPSCs (Figures S2E–S2I). Although blockade of mIPSCs once again increased *Bdnf* and *Npas4* mRNA, increasing excitatory signaling at rest with CX614 had no effect after either 6 h (Figures 2K and 2L) or 30 min (Figures S1D–S1E), ruling out a role for AMPAR current in late and early stages of transcription. Furthermore, reducing excitatory signaling by blocking AMPARs with CNQX also had no effect (Figures 2M and 2N). We then tested the second possibility by using the well-characterized $GABA_AR$ agonist muscimol to increase inhibition at rest. Increased $GABA_AR$ current at rest decreased *Bdnf* and *Npas4* expression (Figures 2O and 2P). We therefore hypothesize that neurons sense inhibition at rest and adjust *Bdnf* and *Npas4* levels accordingly, rather than sensing direct summation of excitatory and inhibitory currents.

Blocking mIPSCs increases calcium signaling at synapses and soma

The effects of fine-tuning mIPSCs on *Bdnf* and *Npas4* transcription suggest a signaling mechanism originating from the synapse. Evoked dendritic inhibition is known to affect local calcium signaling at excitatory synapses, and calcium signaling is strongly linked to transcription of activity-induced genes, including *Bdnf* and *Npas4* (Bengtson et al., 2013; Chiu et al., 2013; Cichon and Gan, 2015; Hayama et al., 2013; Kanemoto et al., 2011, Müllner et al., 2015; Bading, 2013; Flavell and Greenberg, 2008; Lin et al., 2008; Tao et al., 1998; Brigidi et al., 2019); therefore, we tested if mIPSCs affect calcium signaling at excitatory synapses. In these experiments, we expressed a PSD95-tagged version of GCaMP6s using lentivirus (Reese and Kavalali, 2015, 2016) in neurons to target it to excitatory postsynaptic densities (Figure 3A). Surprisingly, blocking mIPSCs increased both the frequency and area of spontaneous calcium transients (SCTs) detected at excitatory synapses (Figures 3B–3D). This increase could be prevented by blocking a major source of calcium influx at excitatory synapses, N-methyl-D-aspartate receptors (NMDARs), with AP5 (Figures 3B–3D). To determine if the synaptic increase in SCTs also translated to a somatic increase in SCTs, we expressed a soluble version of GCaMP6s using lentivirus (Figure 3E). As observed at synapses, blocking mIPSCs increased both the frequency and area of SCTs at the soma (Figures 3F–3H). Notably, this was also blocked by AP5, suggesting that increased calcium signaling is integrated across the dendrites into a somatic response. This notion was corroborated by the observation that increases in SCTs at synapses precede those in the soma (Figure 3I). L-type voltage-gated calcium channels (VGCCs) may mediate the integration of transcription-inducing calcium signals across the dendrites and soma (Wild et al., 2019). Although previously published data demonstrate that L-type VGCCs have no impact on synaptic SCTs (Reese and Kavalali, 2015), we found that the L-type VGCC antagonist, nimodipine, blocked the increase in SCTs at the soma (TTX, 0.1651 ± 0.031 events/min; TTX/PTX/nimodipine, 0.1727 ± 0.034 events/min; paired t test $t_{(29)} = 0.1575$, p = 0.8760, n = 30). These data are consistent with a previous report that calcium signaling from evoked synaptic input is carried by NMDARs and L-type VGCCs (Bengtson et al., 2013) and suggest that NMDARs and L-type VGCCs work together to integrate synaptic and somatic calcium signaling following mIPSC block. The link between mIPSC blockade and increased calcium signaling at cell bodies is neuron-specific, as the addition of PTX did not alter SCTs detected in astrocytes (Figures S3A and S3B).

To understand whether increases in calcium signaling are related to increases in gene transcription following mIPSC blockade, we examined the transcriptional effects of blocking synaptic sources of calcium in addition to mIPSCs. In agreement with our previous findings, a 6-h blockade of mIPSCs led to an increase in *Bdnf* and *Npas4* expression. Blockade of AMPARs with CNQX was unable to prevent this increase in transcription, supporting the premise that excitatory current through AMPARs does not impact gene transcription at rest. However, blocking NMDARs with AP5 or L-type VGCCs with nimodipine abolished this increase in gene transcription (Figures 3J, 3K, and S3K–S3N). Importantly, both NMDARs and L-type VGCCs have been previously shown to regulate *Npas4* expression (Brigidi et al., 2019; Lin et al., 2008). Participation of L-type VGCCs is specific, because the potent and selective T-type VGCC antagonist, TTA-A2, did not impact *Bdnf* or *Npas4* mRNA (Figures S3G–S3J). We next examined the endoplasmic reticulum as a non-synaptic source

of calcium and found that blockade of cytoplasmic calcium influx with ryanodine did not impact *Bdnf* or *Npas4* mRNA (Figures S3C–S3F). Accordingly, ryanodine was unable to block an increase in SCTs at the soma following mIPSC block (TTX/ryanodine, 0.0090 ± 0.0090 events/min; TTX/PTX/ryanodine, 0.0590 ± 0.016 events/min; paired t test $t_{(21)}$ = 2.809, p = 0.0105, n = 22). Taken together, these data suggest that spontaneous GABAergic neurotransmission can be sensed indirectly via NMDAR and L-type VGCC function at excitatory synapses and the soma, and the resulting calcium signaling plays a key role in regulating the transcript levels of *Bdnf* and *Npas4.*

mIPSC blockade induces synaptic downscaling in a BDNF-dependent manner

BDNF and NPAS4 have known roles in synapse remodeling (Zagrebelsky and Korte, 2014; Fu et al., 2020; Park and Poo, 2013; Kowiański et al., 2018). Therefore, we investigated whether mIPSCs, through their ability to measurably alter transcription of these target genes, impact synaptic strength. We measured miniature excitatory postsynaptic currents (mEPSCs) in pyramidal neurons from hippocampal cultures after an initial 6-h blockade of mIPSCs followed by 18 h of recovery in previously collected conditioned media (24 h total) (Figure 4A). Consistent with a role for mIPSCs in impacting synaptic strength, we found that blocking mIPSCs did not alter mEPSC frequency, but led to multiplicative downscaling of mEPSC amplitudes (Figures 4B–4D). This downscaling was abolished when cells were incubated with the transcriptional blocker actinomycin D (ActD) during mIPSC blockade, indicating that transcription is necessary for this effect. ActD application alone at rest had minimal impact on synaptic strength (Figure S4).

As a transcription factor, NPAS4 mediates its effects on synapses through downstream effector molecules, such as BDNF (Lin et al., 2008). BDNF has a well-known role in regulating synaptic strength, leading to increases in strength over short signaling timescales and decreases in strength over long timescales (Rutherford et al., 1998; Autry et al., 2011; Gideons et al., 2017; Reimers et al., 2014; Corrêa et al., 2012). Therefore, we examined BDNF as an effector molecule for the transcription-dependent downscaling seen following blockade of mIPSCs. An initial 6-h blockade of mIPSCs followed by 18 h of recovery resulted in an increase in BDNF protein (Figures 4E and 4F). Moreover, ActD treatment during mIPSC blockade abolished the increase in BDNF protein (Figure 4F), indicating increased BDNF protein is due to translation of newly transcribed *Bdnf* rather than increased local translation (Autry et al., 2011; Sutton et al., 2004, 2006). We also observed that blocking action potentials for the entire duration of the experiment with TTX did not prevent the increase in BDNF protein (Figure 4G), showing that BDNF expression is altered by subthreshold activity-independent signaling. Because mIPSC block leads to a decrease in synaptic strength, and BDNF—which can alter synaptic strength—is increased following mIPSC block, we tested the involvement of BDNF in mIPSC-induced downscaling. In these experiments, we utilized tropomyosin receptor kinase B (TrkB)-immunoglobulin G (IgG) fusion proteins as BDNF scavengers (Nelson et al., 2008). mEPSC frequency was not altered by the inclusion of IgG control protein or TrkB-IgG BDNF-scavenging protein in the replacement conditioned media (Figures 4H and 4I). However, although inclusion of IgG control protein did not affect downscaling following mIPSC block, scavenging BDNF with the TrkB-IgG protein prevented downscaling (Figures 4H and 4J). Collectively, these data

demonstrate that mIPSCs can regulate synaptic strength by altering transcription of *Bdnf,* which is then translated and feeds back onto downregulation of excitatory synaptic function.

DISCUSSION

Previous studies imply an independent function for spontaneous inhibitory signaling through partial segregation of evoked and spontaneous neurotransmission at both pre- and postsynaptic inhibitory specializations (Chung et al., 2010; Horvath et al., 2020). In this study, we identified a role for spontaneous miniature inhibitory neurotransmission in regulating BDNF and excitatory synaptic weights at rest. Importantly, this mechanism is such that it could maintain E/I balance, with a decrease in spontaneous inhibitory events leading to a decrease in excitatory synaptic strength.

We found that the expression of *Bdnf* and *Npas4*, which are typically thought of as activity sensors, is modified in meaningful ways by subthreshold (below action potential threshold) signaling. This is demonstrated by increases in both *Bdnf* and *Npas4* mRNA and BDNF protein in experiments conducted entirely in TTX. These data are also in line with a previous study demonstrating a specific role for synaptic signaling in the regulation of *Npas4* (Brigidi et al., 2019). BDNF signaling induced by mIPSC blockade—dependent on *de novo* BDNF transcription—led to downscaling of excitatory synapses, in agreement with previous data that blockade of subthreshold NMDAR currents can alter BDNF translation-mediated signaling and synaptic strength (Nosyreva et al., 2013). Specifically, decreased subthreshold NMDAR-mediated calcium signaling leads to synaptic upscaling via a short-term increase in BDNF signaling (Nosyreva et al., 2013; Reese and Kavalali, 2015), and increased subthreshold NDMAR-mediated calcium signaling leads to synaptic downscaling via a long-term increase in BDNF signaling (this paper). These data suggest that BDNF not only alters synapse function as an activity sensor per se but also more broadly tunes synapse strength in response to synaptic perturbations.

We propose one mechanism whereby mIPSCs regulate transcription is through calcium signaling at excitatory synapses. Similarly to excitation, inhibitory inputs affect dendritic calcium signaling and long-term synaptic plasticity (Chen et al., 2015; Chiu et al., 2013; Cichon and Gan, 2015; Hayama et al., 2013; Kanemoto et al., 2011; Müllner et al., 2015; Steele and Mauk, 1999). Our work indicates that calcium signaling at excitatory synapses can be altered by mIPSCs even in the absence of somatic spiking. This observation is consistent with the earlier demonstration that inhibition can regulate branch-specific long-term potentiation (LTP), indicating its ability to exert very local effects (Cichon and Gan, 2015; Chen et al., 2015). Changes in local calcium signaling can then be integrated at the soma in order to affect transcription. The length and pattern of calcium signaling alters both the activation of downstream effector molecules and the specific set of activity-induced genes that are transcribed (Tyssowski et al., 2018; Wu et al., 2001; Dolmetsch et al., 1998; Worley et al., 1993). Furthermore, some genes are broadly tuned to respond to a variety of stimuli (Joo et al., 2016). Thus, the specific set of genes transcribed depends heavily on the stimulus and the molecular events that follow. Here, we offer a proof of concept by demonstrating a clear effect of mIPSCs on the transcription of *Bdnf* and its transcription factor *Npas4.* Our experiments suggest a clear functional role for BDNF in regulation of

synaptic strength under these resting conditions, although it must be noted that other genes are also impacted by mIPSC signaling (Figures 1H and 1I). Validating these gene changes and determining the full contributions of this gene set to neuronal functioning will be the focus of future work.

One benefit of examining mIPSCs is that this allowed us to look specifically at the synaptic contribution of inhibition to transcription without confounding increases in network activity or artificial stimulation. Importantly, transcription of *Bdnf* and *Npas4* was bidirectionally modified by inhibitory events, but unaltered by manipulations of quantal AMPAR-mediated events, the main carrier of excitatory currents at rest. This indicates that in addition to shaping fast excitatory currents and somatic spiking (Bloss et al., 2016; Iascone et al., 2020), inhibition also has a role in shaping the slower and longer lasting molecular signaling of a neuron. Thus, brain regions that are primarily composed of inhibitory interneurons (i.e., striatum and medial amygdala) may not only represent passive relay centers functioning as fast off- or on-switches, but may transform information processing by affecting molecular signaling and synaptic plasticity in downstream neurons. In agreement with this broader role for inhibition, it has recently been shown that complex behaviors, such as parenting and feeding, are controlled by subsets of inhibitory neurons (Wu et al., 2014; Aponte et al., 2011; Vong et al., 2011). Delineating the extent of evoked and spontaneous miniature inhibitory neurotransmission's role in molecular signaling will be necessary to gain a full picture of inhibition's role in the brain.

STAR★METHODS

RESOURCE AVAILABILITY

Lead contact—Further information and requests for resources and reagents should be directed to and will be fulfilled by the Lead Contact, Lisa M. Monteggia (Lisa.Monteggia@vanderbilt.edu).

Materials availability—This study did not generate new unique reagents.

Data and code availability

- Bulk RNA-sequencing data have been deposited at NCBI's Sequence Read Archive (SRA) and are publicly available as of the date of publication. Accession numbers are listed in the Key Resources Table. All data reported in this paper will be shared by the lead contact upon request.
- This paper does not report original code.
- Any additional information required to reanalyze the data reported in this paper is available from the lead contact upon request.

EXPERIMENTAL MODEL AND SUBJECT DETAILS

Animals—Sprague-Dawley rat pups (postnatal day 1-3, Charles River, strain code: 400) of both sexes were used for all experiments. PN1-3 littermates were used to prepare primary, mixed-sex, dissociated, neuronal cultures. Pregnant Sprague-Dawley dams were

housed individually. The rats were kept in a 12hrs:12hrs dark:light cycle. Animal procedures conformed to the Guide for the Care and Use of Laboratory Animals and were approved by the Institutional Animal Care and Use Committees at UT Southwestern Medical Center and Vanderbilt University. Health status of live animals was periodically checked and confirmed by the veterinary staff of the animal facilities at UT Southwestern Medical Center and Vanderbilt University.

Primary Dissociated Hippocampal Culture—Dissociated hippocampal cultures were prepared as previous described (Kavalali et al., 1999). Sex was not determined before culturing, and all cultures consisted of neurons from mixed sexes. Whole hippocampi were dissected from PN1-3 rats, trypsinized (~4 mg/mL, Sigma), treated with DNase I, mechanically dissociated, and plated on matrigel (BD Biosciences) coated plastic or glass coverslips. Neurons were plated in MEM (no phenol red) containing 27.8 mM of Glucose, 2.4 mM of $NaHCO_3$, 1.3 μM of Transferrin (Calbiochem), 2 mM of L-Glutamine, 4.4 μM of insulin, and 10% FBS. On DIV1, FBS concentration was reduced to 5%, L-Glutamine concentration was reduced to 500 μM, and 1x B-27 supplement (GIBCO) and 4μM of cytosine arabinoside (ARAC; Sigma) were added. On DIV4 the concentration of ARAC was reduced to 2μM. For imaging experiments, cells were also infected on DIV4 with 100 μL of lentivirus carrying either a GCaMP6s or GCaMP6s-PSD95 expression plasmid. Cells were maintained at 37°C in a 5% CO_2 atmosphere without disruption following DIV4 until experiments were performed (DIV14-21). Sample size was not predetermined using statistical methods prior to experimentation. Sample sizes were based on previous studies in the field of molecular & cellular neuroscience.

Cell lines—Human embryonic kidney-293 (HEK293-T) cells (authenticated by ATCC) were used to produce lentiviral particles to infect primary neuronal cultures. HEK293 cultures were maintained in Dulbecco's Modified Eagle Medium supplemented with 10% FBS, penicillin, and streptavidin at 37°C in a 5% CO_2 atmosphere. Cells were split and passaged when they reached 80% confluency. Cultures with more than 30 passages were not used.

METHOD DETAILS

Cloning and Lentivirus production—GCaMP6s was subcloned into FUGW and FUGW-GCaMP6f-PSD95 (replacing GFP and GCaMP6f, respectively) using classic molecular biology techniques (Chen et al., 2013; Lois et al., 2002; Reese and Kavalali, 2016). HEK293-T cells were transfected with FuGENE6, necessary viral coat and packaging protein constructs (pCMV-VSV-G, pMDLg-pRRE, pRSV-Rev), and either a GCaMP6sor GCaMP6s-PSD95 expression plasmid (Dull et al., 1998; Stewart et al., 2003). 12-18 hr after transfection, HEK293-T cell media was replaced with MEM (no phenol red) media containing 5% FBS, 500 μM L-glutamine and 1x B-27 supplement (GIBCO). On DIV3 virus was harvested from the HEK293-T cell media and added directly to neuronal media at DIV4.

Electrophysiology—Electrophysiology was performed on cells from DIV15-21 at room temperature using a CV 203BU headstage (Axon Instruments), Axopatch 200B amplifier,

Digidata 1322A digitizer and Clampex 10 software (Molecular Devices). Extracellular Tyrode solution, adjusted to pH 7.4 and 319 mOsm, contained: 150 mM of NaCl, 4 mM of KCl, 1.25 mM of $MgCl_2 \cdot 6H_2O$, 10 mM of glucose, 10 mM of HEPES, 2 mM of Ca^{2+}, and 1 μM of tetrodotoxin (TTX). For whole cell patch voltage clamp recordings, 50 μM of D-AP5 and 50 μM of picrotoxin (PTX) was added to the extracellular solution to isolate α-amino-3-hydroxy-5-methyl-4-isoxazolepropionic acid (AMPA) driven miniature excitatory postsynaptic currents (mEPSCs) and 50μM of D-AP5, and 10μM of NBQX was added to isolate miniature inhibitory postsynaptic currents (mIPSCs). Intracellular pipette solution for voltage clamp recordings, adjusted to pH 7.3 and 304 mOsm, contained: 115 mM of Cs-methanesulphonate, 10 mM of CsCl, 5 mM of NaCl, 10 mM of HEPES, 20 mM of TEA.Cl hydrate, 4 mM of MgATP, 0.3 mM of GTP, 0.6 mM of EGTA, and 10 mM of QX314. For whole cell patch current clamp recordings 50 μM of PTX was added to extracellular solution where indicated. Intracellular pipette solution for current clamp recordings, adjusted to pH 7.3 and 304 mOsm, contained: 138 mM of Kgluconate, 2 mM of NaCl, 2 mM of NaCl, 0.3 mM of Tris-GTP, 4 mM of Mg_2ATP, 14 mM of (di)Trisphosphocreatine, and 10 mM of HEPES. For synaptic scaling experiments, 6 hr after initial drug treatment with 1 μM of TTX, 50 μM of PTX, and/or 2.5 μM of ActD, drug-treated media was replaced with conditioned media (collected before drug treatment) and returned to the incubator for 18 hr. In BDNF-scavenging experiments, conditioned replacement media was treated with either 12.5μg/mL IgG control, or 12.5μg/mL TrkB-IgG. mEPSCs were then recorded as described, 24 hr after the start of the experiment. To calculate membrane input resistance, current steps of 20 pA were given and the resulting potential was plotted against the current injection and fitted with a line. Input resistance was calculated from the slope of this line. Series resistance was monitored before and after all recordings to ensure stable patches. Series resistance compensation was not employed in these recordings. In cases where multiple files were recorded from the same patch, series resistance was monitored in between each file. Liquid junction potential was not corrected for in these recordings. Spontaneous excitatory and inhibitory currents and potentials were analyzed using MiniAnalysis software with the analyzer blind to experimental condition. Recordings were made from cells across multiple coverslips from at least two independent cultures with every condition represented in each culture for each experiment to ensure adequate biological and technical replication.

Drug treatment and RNA collection—Dissociated hippocampal cultures (DIV14) were treated as indicated in figures for 6 hr or 30 min. The following drugs were used at the indicated concentrations: TTX (1 μM), PTX (50 μM), Bicuculline (20 μM), CX614 (20 μM), CNQX (10 μM), AP5 (50 μM), Muscimol (5 μM), Nimodipine (5 μM), Ryanodine (33 μM), TTA-A2 (10 μM). All drugs and vehicle controls were added directly to cell media. Following drug treatment, media was aspirated, cells were lysed, and RNA was collected using the PureLink® RNA mini kit with supplementary DNase treatment (Thermo Fisher Scientific) according to manufacturer instructions. RNA was eluted with 40 μL of nuclease-free H_2O. RNA was collected from individual wells from at least three independent cultures with every condition represented in each culture for each experiment to ensure adequate biological and technical replication.

cDNA preparation and qPCR—400 ng of RNA was converted to cDNA using the SuperScript® III Reverse Transcriptase kit (Thermo Fisher Scientific) according to manufacturer specifications. Briefly, RNA was mixed with 1x random primer and 10mM dNTPs then incubated at 65°C for 5 minutes. 5x First Strand Buffer, 100mM DTT and RNase out were then added and the reaction mixture was incubated at 25°C for 5 minutes. Finally, the reverse transcriptase (SSIII) was added and the reaction was incubated at 50°C for 1 hr followed by 70°C for 15 minutes.

cDNA was then used for qPCR according to the following mixture: 10 μL of Power *SYBR*® Green PCR Master Mix (Thermo Fisher Scientific), 7 μL of nuclease-free H2O,1 μL of forward primer (10μM), 1 μL of reverse primer (10μM), and 1μL of cDNA. Forward and reverse primer sequences for each gene assayed are listed in the Key Resources Table. The qPCR reaction was performed in triplicate for each sample according to the following temperature profile: (1) 95°C for 10 minutes, (2) 95°C for 30 s, (3) 60°C for 20 s, (4) 70°C for 30 s, steps 2-4 were repeated for 40 cycles. All Ct values were normalized to *Gapdh* and analyzed using the standard curve method.

Western Blotting—On DIV14, cells were treated as indicated in figures. The following drugs were used at the indicated concentrations: TTX (1 μM), PTX (50 μM), and ActD (2.5 μM). All drugs and vehicle controls were added directly to cell media. For 24 hr experiments, 6 hr after initial drug treatment, drug-treated media was replaced with conditioned media (collected before drug treatment) and returned to the incubator for 18 hr. 24 hr after initial drug treatment, cells were collected in 75μL PBS and 75μL Laemmli sample buffer (BioRad) containing protease and phosphatase inhibitors (Roche). 30μL of cell lysate was run on an SDS/PAGE gel and then transferred to a nitrocellulose membrane using the Trans-Blot Turbo transfer system (BioRad). Following 30 min in blocking solution, primary antibodies were used at the following concentrations: GAPDH 1:50,000; BDNF 1:1,500; ERK 1:2,000; pERK 1:2,000; CREB 1:2,000; pCREB 1:5,000. After incubation in primary antibodies at 4°C overnight, membranes were incubated in secondary antibodies at the following concentrations: GAPDH 1:10,000 (anti-rabbit); BDNF, ERK, pERK, CREB, and pCREB 1:5,000 (anti-rabbit). Protein bands were detected using ECL and exposure to film. Quantification was performed using ImageJ to detect protein band intensities. Values were normalized to GAPDH before comparison. Protein/cell lysate was collected from individual wells from at least two independent cultures with every condition represented in each culture for each experiment to ensure adequate biological and technical replication.

Live cell Calcium imaging—Cultured hippocampal neurons were infected on DIV4 with lentivirus containing either GCaMP6s or GCaMP6s-PSD95 and then imaged on DIV18-20. Tyrode's buffer adjusted to pH 7.4 and 319 mOsm, containing 150 mM of NaCl, 4 mM of KCl, 10 mM of glucose, 10 mM of HEPES, 2 mM of Ca^{2+} and 1.25 mM of Mg^{2+} with 1 μM of TTX and, when appropriate, 50 μM of PTX, 50 μM of D-AP5, 33 μM of Ryanodine, and/or 5 μM of Nimodipine was used. Experiments were performed with constant perfusion and at room temperature using a Nikon Eclipse TE2000-U microscope (Nikon) equipped with a Lambda-DG4 illumination system (Sutter instruments), a FITC

emission filter and a 60x (1.4 NA) objective. Images were acquired at 7 Hz using an Andor iXon+ back-illuminated EMCCD camera (Model no. DU-897E-CSO-#BV). Maximal fluorescence signal was obtained by perfusion of 90 mM of KCl at the end of each experiment and this was used to draw the regions of interest (ROI) around postsynaptic spines, dendrites and cell bodies. Spontaneous calcium transients (SCTs) were measured from ROIs for 5min before and for 10 min immediately after addition of drugs. Images and fluorescence values were analyzed using Fiji (Schindelin et al., 2012) and MATLAB. Images were collected from individual coverslips from at least two independent cultures with every condition represented in each culture for each experiment to ensure adequate biological and technical replication.

RNA-sequencing and analysis—Dissociated hippocampal cultures were treated with DMSO vehicle, 50 μM PTX and/or 1 μM TTX for 6 hr to create basal, PTX, TTX, and TTX/PTX groups. Following drug incubation, total RNA was collected from 2 wells per condition in two independent cultures for a total of 4 samples per group to ensure adequate biological and technical replication. RNA was collected via the RNeasy Plus Mini Kit (QIAGEN) according to manufacturer instructions. A Quality Control assessment was completed for the total RNA utilizing a Qubit RNA assay to quantify each sample and the Caliper GX to evaluate integrity. All samples had an RNA integrity number (RIN) above 8.6. RNASeq libraries were prepared using 300 ng of RNA and the NEBNext Ultra II Directional RNA Library Prep kit (NEB, Cat: E7760L). Fragmentation, cDNA synthesis, end repair/dA-tailing, adaptor ligation and PCR enrichment were performed per manufacturer's instructions. Individual libraries were assessed for quality using the Agilent 2100 Bioanalyzer and quantified with a Qubit Fluorometer. The adaptor ligated material was evaluated using qPCR prior to normalization and pooling for sequencing. The libraries were sequenced using the NovaSeq 6000 with 150 bp paired end reads. RTA (version 2.4.11; Illumina) was used for base calling and data QC was completed using MultiQC v1.7 by the Vanderbilt Technologies for Advanced Genomics (VANTAGE) core (Vanderbilt University, Nashville, TN). For sequencing analysis, adapters were trimmed by Cutadapt (v2.10). After trimming, reads were mapped to the rat genome Rnor 6.0 using STAR (v2.7.8a) and quantified by feature Counts (v2.0.2). DESeq2 (v.1.30.1) was used to detect differential expression between two groups. Fold change of at least 1.5 in either direction compared to control was used as the cut-off. Adjusted p values less than 0.05 were considered statistically significant.

QUANTIFICATION AND STATISTICAL ANALYSIS

All statistical analyses were performed using GraphPad Prism 8 software. Details on statistical tests performed and n for each experiment are listed in Table S1. For RNA and protein experiments n is one individual well of neurons from a cultured set. For electrophysiology experiments n is one patched cell. For imaging experiments frequency n is each individual ROI corresponding to either a single synapse or cell body and area n is each individual event across ROIs in all samples. Sample size was not predetermined using statistical methods prior to experimentation. Sample sizes were based on previous studies in the field of molecular & cellular neuroscience. Outliers were identified with the Robust regression and Outlier removal (ROUT) method. Statistical significance was defined as p

< 0.05 with further details listed in Table S1 for main figures and in figure legends for supplemental figures.

Supplementary Material

Refer to Web version on PubMed Central for supplementary material.

ACKNOWLEDGMENTS

The contents of this publication are solely the responsibility of the authors and do not necessarily represent the official views of NIGMS, NIH, or VBI. Graphical abstract created with BioRender.com by Natalie J. Guzikowski. This work was supported by NIH (GM008203 to P.M.H., MH081060 and MH070727 to L.M.M., and MH066198 to E.T.K.), by a NARSAD Young Investigator Grant (to N.L.C.), and by the Vanderbilt Brain Institute (VBI) Trans-Institutional Programs (600658 to B.A.).

REFERENCES

Aponte Y, Atasoy D, and Sternson SM (2011). AGRP neurons are sufficient to orchestrate feeding behavior rapidly and without training. Nat. Neurosci. 14, 351–355. [PubMed: 21209617]

Arai AC, Kessler M, Rogers G, and Lynch G (2000). Effects of the potent ampakine CX614 on hippocampal and recombinant AMPA receptors: interactions with cyclothiazide and GYKI 52466. Mol. Pharmacol. 58, 802–813. [PubMed: 10999951]

Autry AE, and Monteggia LM (2012). Brain-derived neurotrophic factor and neuropsychiatric disorders. Pharmacol. Rev. 64, 238–258. [PubMed: 22407616]

Autry AE,Adachi M, Nosyreva E, Na ES, Los MF, Cheng PF, Kavalali ET, and Monteggia LM (2011). NMDA receptor blockade at rest triggers rapid behavioural antidepressant responses. Nature 475, 91–95. [PubMed: 21677641]

Bading H (2013). Nuclear calcium signalling in the regulation of brain function. Nat. Rev. Neurosci. 14, 593–608. [PubMed: 23942469]

Bengtson CP, Kaiser M, Obermayer J, and Bading H (2013). Calcium responses to synaptically activated bursts of action potentials and their synapse-independent replay in cultured networks of hippocampal neurons. Biochim. Biophys. Acta 1833, 1672–1679. [PubMed: 23360982]

Bito H, Deisseroth K, and Tsien RW (1996). CREB phosphorylation and dephosphorylation: a Ca(2+)- and stimulus duration-dependent switch for hippocampal gene expression. Cell 87, 1203–1214. [PubMed: 8980227]

Bloss EB, Cembrowski MS, Karsh B, Colonell J, Fetter RD, and Spruston N (2016). Structured Dendritic Inhibition Supports Branch-Selective Integration in CA1 Pyramidal Cells. Neuron 83, 1016–1030.

Brigidi GS, Hayes MGB, Delos Santos NP, Hartzell AL, Texari L, Lin PA, Bartlett A, Ecker JR, Benner C, Heinz S, and Bloodgood BL (2019). Genomic Decoding of Neuronal Depolarization by Stimulus-Specific NPAS4 Heterodimers. Cell 173, 373–391.e27.

Chen TW, Wardill TJ, Sun Y, Pulver SR, Renninger SL, Baohan A, Schreiter ER, Kerr RA, Orger MB, Jayaraman V, et al. (2013). Ultrasensitive fluorescent proteins for imaging neuronal activity. Nature 433, 295–300.

Chen SX, Kim AN, Peters AJ, and Komiyama T (2015). Subtype-specific plasticity of inhibitory circuits in motor cortex during motor learning. Nat. Neurosci. 18, 1109–1115. [PubMed: 26098758]

Chiu CQ, Lur G, Morse TM, Carnevale NT, Ellis-Davies GC, and Higley MJ (2013). Compartmentalization of GABAergic inhibition by dendritic spines. Science 340, 759–762. [PubMed: 23661763]

Chung C, Barylko B, Leitz J, Liu X, and Kavalali ET (2010). Acute dynamin inhibition dissects synaptic vesicle recycling pathways that drive spontaneous and evoked neurotransmission. J. Neurosci. 30, 1363–1376. [PubMed: 20107062]

Cichon J, and Gan WB (2015). Branch-specific dendritic Ca(2+) spikes cause persistent synaptic plasticity. Nature 520, 180–185. [PubMed: 25822789]

Corrêa SA, Hunter CJ, Palygin O, Wauters SC, Martin KJ, McKenzie C, McKelvey K, Morris RG, Pankratov Y, Arthur JS, and Frenguelli BG (2012). MSK1 regulates homeostatic and experience-dependent synaptic plasticity. J. Neurosci. 32, 13039–13051. [PubMed: 22993422]

Dienel SJ, and Lewis DA (2019). Alterations in cortical interneurons and cognitive function in schizophrenia. Neurobiol. Dis. 131, 104208. [PubMed: 29936230]

Dolmetsch RE, Xu K, and Lewis RS (1998). Calcium oscillations increase the efficiency and specificity of gene expression. Nature 332, 933–936.

Dull T, Zufferey R, Kelly M, Mandel RJ, Nguyen M, Trono D, and Naldini L (1998). A third-generation lentivirus vector with a conditional packaging system. J. Virol. 72, 8463–8471. [PubMed: 9765382]

Duman RS, and Monteggia LM (2006). A neurotrophic model for stress-related mood disorders. Biol. Psychiatry 53, 1116–1127.

Duman RS, Sanacora G, and Krystal JH (2019). Altered Connectivity in Depression: GABA and Glutamate Neurotransmitter Deficits and Reversal by Novel Treatments. Neuron 102, 75–90. [PubMed: 30946828]

Flavell SW, and Greenberg ME (2008). Signaling mechanisms linking neuronal activity to gene expression and plasticity of the nervous system. Annu. Rev. Neurosci. 31, 563–590. [PubMed: 18558867]

Fu J, Guo O, Zhen Z, and Zhen J (2020). Essential Functions of the Transcription Factor Npas4 in Neural Circuit Development, Plasticity, and Diseases. Front. Neurosci. 14, 603373. [PubMed: 33335473]

Funahashi Y, Ariza A, Emi R, Xu Y, Shan W, Suzuki K, Kozawa S, Ahammad RU, Wu M, Takano T, et al. (2019). Phosphorylation of Npas4 by MAPK Regulates Reward-Related Gene Expression and Behaviors. Cell Rep. 29, 3235–3252.e9. [PubMed: 31801086]

Gideons ES, Lin PY, Mahgoub M, Kavalali ET, and Monteggia LM (2017). Chronic lithium treatment elicits its antimanic effects via BDNF-TrkB dependent synaptic downscaling. eLife 6, e25480. [PubMed: 28621662]

Hayama T, Noguchi J, Watanabe S, Takahashi N, Hayashi-Takagi A, Ellis-Davies GC, Matsuzaki M, and Kasai H (2013). GABA promotes the competitive selection of dendritic spines by controlling local Ca2+ signaling. Nat. Neurosci. 16, 1409–1416. [PubMed: 23974706]

Horvath PM, Piazza MK, Monteggia LM, and Kavalali ET (2020). Spontaneous and evoked neurotransmission are partially segregated at inhibitory synapses. eLife 9, e52852. [PubMed: 32401197]

Iascone DM, Li Y, Sümbül U, Doron M, Chen H, Andreu V, Goudy F, Blockus H, Abbott LF, Segev I, et al. (2020). Whole-Neuron Synaptic Mapping Reveals Spatially Precise Excitatory/Inhibitory Balance Limiting Dendritic and Somatic Spiking. Neuron 106, 566–578.e8. [PubMed: 32169170]

Joo JY, Schaukowitch K, Farbiak L, Kilaru G, and Kim TK (2016). Stimulus-specific combinatorial functionality of neuronal c-fos enhancers. Nat. Neurosci. 19, 75–83. [PubMed: 26595656]

Kalueff AV, and Nutt DJ (2007). Role of GABA in anxiety and depression. Depress. Anxiety 24, 495–517. [PubMed: 17117412]

Kanemoto Y, Matsuzaki M, Morita S, Hayama T, Noguchi J, Senda N, Momotake A, Arai T, and Kasai H (2011). Spatial distributions of GABA receptors and local inhibition of Ca2+ transients studied with GABA uncaging in the dendrites of CA1 pyramidal neurons. PLoS ONE 6, e22652. [PubMed: 21799926]

Kavalali ET (2015). The mechanisms and functions of spontaneous neurotransmitter release. Nat. Rev. Neurosci. 16, 5–16. [PubMed: 25524119]

Kavalali ET, Klingauf J, and Tsien RW (1999). Activity-dependent regulation of synaptic clustering in a hippocampal culture system. Proc. Natl. Acad. Sci. USA 96, 12893–12900. [PubMed: 10536019]

Kowiański P, Lietzau G, Czuba E, Waśkow M, Steliga A, and Moryś J (2018). BDNF: A Key Factor with Multipotent Impact on Brain Signaling and Synaptic Plasticity. Cell. Mol. Neurobiol. 38, 579–593. [PubMed: 28623429]

Li B, Suutari BS, Sun SD, Luo Z, Wei C, Chenouard N, Mandelberg NJ, Zhang G, Wamsley B, Tian G, et al. (2020). Neuronal Inactivity Coopts LTP Machinery to Drive Potassium Channel Splicing and Homeostatic Spike Widening. Cell 181, 1547–1565.e15. [PubMed: 32492405]

Lin Y, Bloodgood BL, Hauser JL, Lapan AD, Koon AC, Kim TK, Hu LS, Malik AN, and Greenberg ME (2008). Activity-dependent regulation of inhibitory synapse development by Npas4. Nature 455, 1198–1204. [PubMed: 18815592]

Lois C, Hong EJ, Pease S, Brown EJ, and Baltimore D (2002). Germline transmission and tissue-specific expression of transgenes delivered by lentiviral vectors. Science 295, 868–872. [PubMed: 11786607]

Marín O (2012). Interneuron dysfunction in psychiatric disorders. Nat. Rev. Neurosci. 13, 107–120. [PubMed: 22251963]

Müllner FE, Wierenga CJ, and Bonhoeffer T (2015). Precision of Inhibition: Dendritic Inhibition by Individual GABAergic Synapses on Hippocampal Pyramidal Cells Is Confined in Space and Time. Neuron 87, 576–589. [PubMed: 26247864]

Nelson ED, Kavalali ET, and Monteggia LM (2008). Activity-dependent suppression of miniature neurotransmission through the regulation of DNA methylation. J. Neurosci. 28, 395–406. [PubMed: 18184782]

Nosyreva E, Szabla K, Autry AE, Ryazanov AG, Monteggia LM, and Kavalali ET (2013). Acute suppression of spontaneous neurotransmission drives synaptic potentiation. J. Neurosci. 33, 6990–7002. [PubMed: 23595756]

Obrietan K, Gao XB, and Van Den Pol AN (2002). Excitatory actions of GABA increase BDNF expression via a MAPK-CREB-dependent mechanism-a positive feedback circuit in developing neurons. J. Neurophysiol. 88, 1005–1015. [PubMed: 12163549]

Park H, and Poo MM (2013). Neurotrophin regulation of neural circuit development and function. Nat. Rev. Neurosci. 14, 7–23. [PubMed: 23254191]

Reese AL, and Kavalali ET (2015). Spontaneous neurotransmission signals through store-driven Ca(2+) transients to maintain synaptic homeostasis. eLife 4, e09262.

Reese AL, and Kavalali ET (2016). Single synapse evaluation of the postsynaptic NMDA receptors targeted by evoked and spontaneous neurotransmission. eLife 5, e21170. [PubMed: 27882871]

Reimers JM, Loweth JA, and Wolf ME (2014). BDNF contributes to both rapid and homeostatic alterations in AMPA receptor surface expression in nucleus accumbens medium spiny neurons. Eur. J. Neurosci. 39, 1159–1169. [PubMed: 24712995]

Rubenstein JL, and Merzenich MM (2003). Model of autism: increased ratio of excitation/inhibition in key neural systems. Genes Brain Behav. 2, 255–267. [PubMed: 14606691]

Rutherford LC, Nelson SB, and Turrigiano GG (1998). BDNF has opposite effects on the quantal amplitude of pyramidal neuron and interneuron excitatory synapses. Neuron 21, 521–530. [PubMed: 9768839]

Schaukowitch K, Reese AL, Kim SK, Kilaru G, Joo JY, Kavalali ET, and Kim TK (2017). An Intrinsic Transcriptional Program Underlying Synaptic Scaling during Activity Suppression. Cell Rep. 18, 1512–1526. [PubMed: 28178527]

Schindelin J, Arganda-Carreras I, Frise E, Kaynig V, Longair M, Pietzsch T, Preibisch S, Rueden C, Saalfeld S, Schmid B, et al. (2012). Fiji: an open-source platform for biological-image analysis. Nat. Methods 9, 676–682. [PubMed: 22743772]

Steele PM, and Mauk MD (1999). Inhibitory control of LTP and LTD: stability of synapse strength. J. Neurophysiol. 81, 1559–1566. [PubMed: 10200191]

Stewart SA, Dykxhoorn DM, Palliser D, Mizuno H, Yu EY, An DS, Sabatini DM, Chen IS, Hahn WC, Sharp PA, et al. (2003). Lentivirus-delivered stable gene silencing by RNAi in primary cells. RNA 9, 493–501. [PubMed: 12649500]

Sutton MA, Wall NR, Aakalu GN, and Schuman EM (2004). Regulation of dendritic protein synthesis by miniature synaptic events. Science 304, 1979–1983. [PubMed: 15218151]

Sutton MA, Ito HT, Cressy P, Kempf C, Woo JC, and Schuman EM (2006). Miniature neurotransmission stabilizes synaptic function via tonic suppression of local dendritic protein synthesis. Cell 125, 785–799. [PubMed: 16713568]

Tao X, Finkbeiner S, Arnold DB, Shaywitz AJ, and Greenberg ME (1998). Ca2+ influx regulates BDNF transcription by a CREB family transcription factor-dependent mechanism. Neuron 20, 709–726. [PubMed: 9581763]

Thomas GM, and Huganir RL (2004). MAPK cascade signalling and synaptic plasticity. Nat. Rev. Neurosci. 5, 173–183. [PubMed: 14976517]

Tyssowski KM, DeStefino NR, Cho JH, Dunn CJ, Poston RG, Carty CE, Jones RD, Chang SM, Romeo P, Wurzelmann MK, et al. (2018). Different Neuronal Activity Patterns Induce Different Gene Expression Programs. Neuron 98, 530–546.e11. [PubMed: 29681534]

Vong L, Ye C, Yang Z, Choi B, Chua S Jr., and Lowell BB (2011). Leptin action on GABAergic neurons prevents obesity and reduces inhibitory tone to POMC neurons. Neuron 71, 142–154. [PubMed: 21745644]

Wild AR, Sinnen BL, Dittmer PJ, Kennedy MJ, Sather WA, and Dell'Acqua ML (2019). Synapse-to-Nucleus Communication through NFAT Is Mediated by L-type Ca^{2+} Channel Ca^{2+} Spike Propagation to the Soma. Cell Rep. 26, 3537–3550.e4. [PubMed: 30917310]

Worley PF, Bhat RV, Baraban JM, Erickson CA, McNaughton BL, and Barnes CA (1993). Thresholds for synaptic activation of transcription factors in hippocampus: correlation with long-term enhancement. J. Neurosci. 13, 4776–4786. [PubMed: 8229198]

Wu GY, Deisseroth K, and Tsien RW (2001). Spaced stimuli stabilize MAPK pathway activation and its effects on dendritic morphology. Nat. Neurosci. 4, 151–158. [PubMed: 11175875]

Wu Z, Autry AE, Bergan JF, Watabe-Uchida M, and Dulac CG (2014). Galanin neurons in the medial preoptic area govern parental behaviour. Nature 509, 325–330. [PubMed: 24828191]

Zagrebelsky M, and Korte M (2014). Form follows function: BDNF and its involvement in sculpting the function and structure of synapses. Neuropharmacology 76, 628–638. [PubMed: 23752094]

Highlights

- Transcription can be directly driven by inhibitory signaling
- At rest, neurons sense inhibition, not summation of excitatory/inhibitory current
- mIPSCs regulate calcium signaling at excitatory synapses and somas
- Blocking mIPSCs downscales excitatory synapses via *Bdnf* transcription and signaling

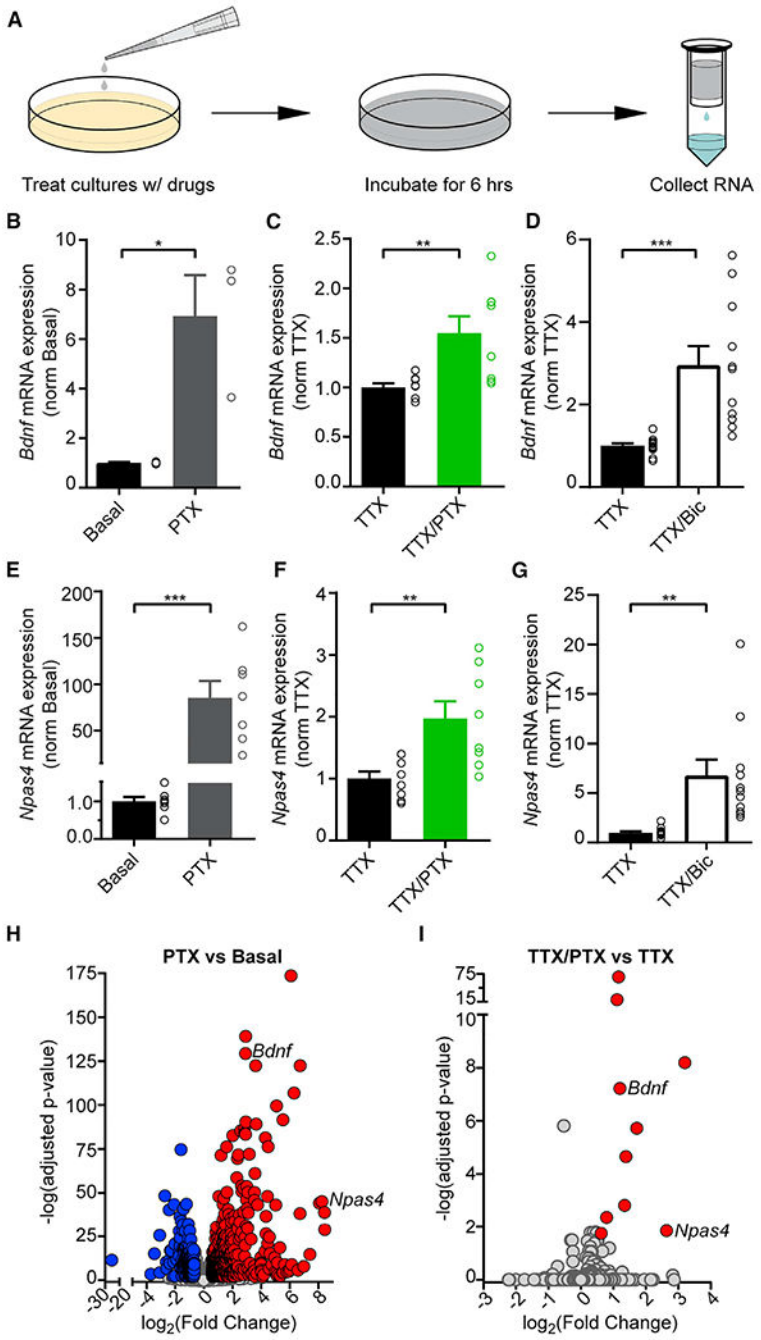

Figure 1. mIPSC block increases *Bdnf* and *Npas4* mRNA

(A) Experimental schematic (B–I). RNA was collected from cultured hippocampal neurons 6 h after drug treatment.

(B and E) Blocking inhibition with 50 μM PTX increases *Bdnf* (B, n = 3) and *Npas4* (E, n = 7) mRNA.

(C and F) Blocking mIPSCs with 1 μM TTX and 50 μM PTX increases *Bdnf* (C) and *Npas4* (F) mRNA (n = 8).

(D and G) Blocking mIPSCs with 1 μM TTX and 20 μM bicuculline increases *Bdnf* (D) and *Npas4* (G) mRNA (TTX, n = 12; TTX/bicuculline, n = 11).
(H) Blocking inhibition with 50 μM PTX leads to differential expression of many genes (DEGs) compared to baseline, including *Bdnf* and *Npas4.*
(I) Blocking mIPSCs with 1 μM TTX and 50 μM PTX increases expression of a small subset of genes compared to 1 μM TTX-treated cells, including *Bdnf* and *Npas4*. RNA-seq experiments had 4 biological replicates. Bar graphs are mean + SEM. Open circles next to bars = biological replicates. Volcano plots show DEGs with increased (red) or decreased (blue) expression. n.s., non-significant, *p < 0.05, **p < 0.01, ***p< 0.001.
See also Figure S1 and Tables S1, S2, and S3.

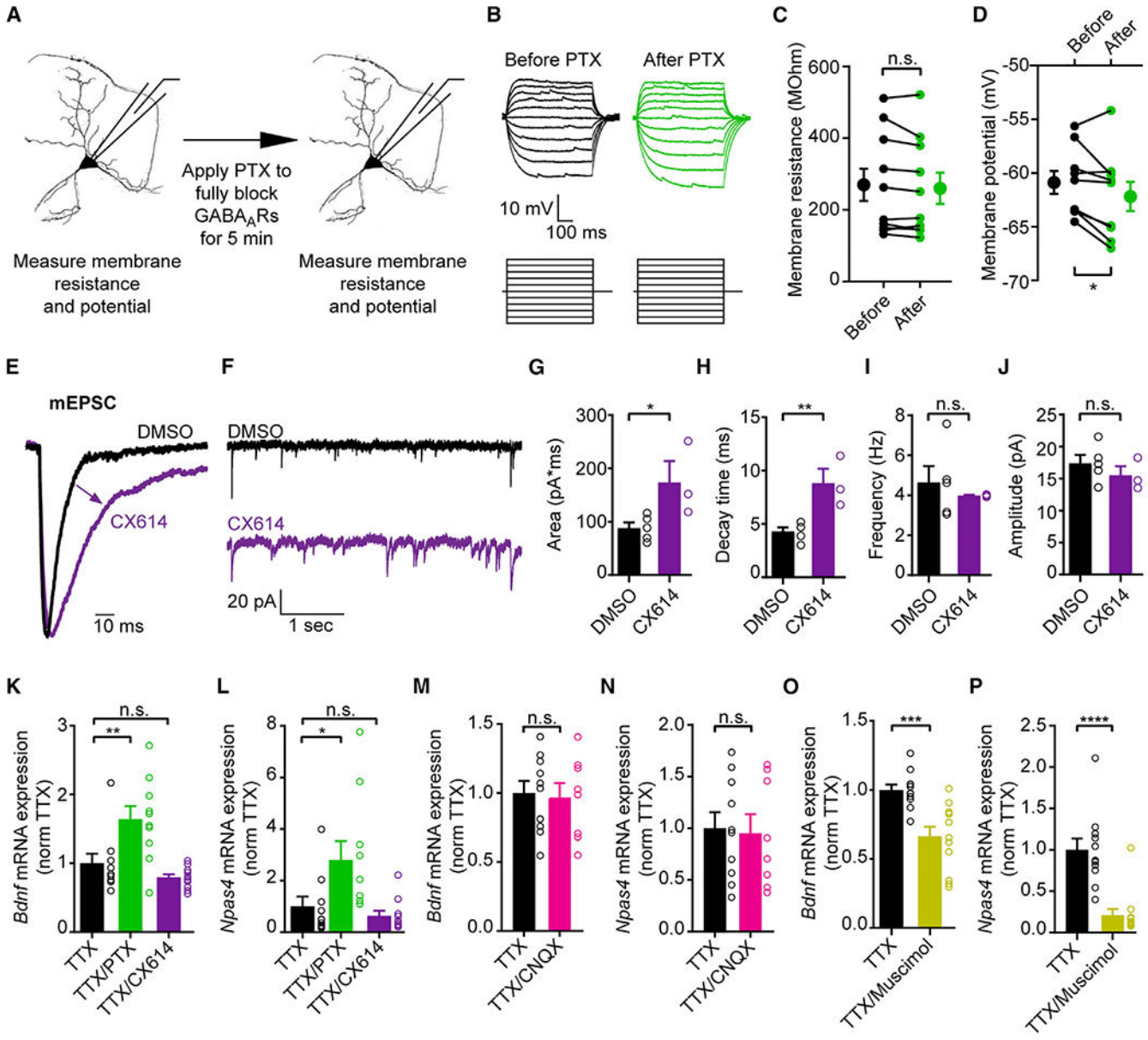

Figure 2. Neurons adjust transcription at rest by sensing inhibitory input not E/I ratio

(A) Experimental schematic (B–D). Pyramidal neurons were whole-cell patched in current (B–D) or voltage clamp (E–J). Current clamp measurements were taken in 1 μM TTX from same cell before and after 5 min incubation with 50 μM PTX. Voltage clamp measurements were taken from different cells with 20 μM CX614 or DMSO in extracellular bath.

(B) Representative traces (C and D).

(C) Membrane resistance is unaltered following mIPSP block with 1 μM TTX and 50 μM PTX (n = 10).

(D) Membrane potential is mildly decreased following mIPSP block with 1 μM TTX and 50 μM PTX (n = 9).

(E) Scaled average mEPSC event in presence or absence of 20 μM CX614.

(F) Representative traces (G–J).

(G–J) 20 μM CX614 increases the area (G) and decay time (H), but does not the affect frequency (I) or amplitude (J) of mEPSCs (DMSO, n = 5; CX614, n = 3).
(K–P) RNA was collected from cultured hippocampal neurons 6 h after drug treatment.
(K and L) Blocking mIPSCs with 1 μM TTX and 50 μM PTX increases *Bdnf* (K) and *Npas4* (L) mRNA, but increasing mEPSC charge transferred with 20 μM CX614 does not (TTX, n = 10; TTX/PTX, n = 10; TTX/CX614, n = 11).
(M and N) Blocking mEPSCs with 10 μM CNQX does not alter *Bdnf* (M) or *Npas4* (N) mRNA (TTX, n = 10; TTX/CNQX, n = 8).
(O and P) Activating $GABA_A$Rs at rest with 5 μM muscimol decreases *Bdnf* (O) and *Npas4* (P) mRNA (TTX, n = 11; TTX/muscimol, n = 12). Large circles in (C) and (D) are mean ± SEM. Bar graphs are mean + SEM. Open circles next to bars = biological replicates. n.s., non-significant, *p < 0.05, **p < 0.01, ***p < 0.001, ****p < 0.0001.
See also Figure S2 and Table S1.

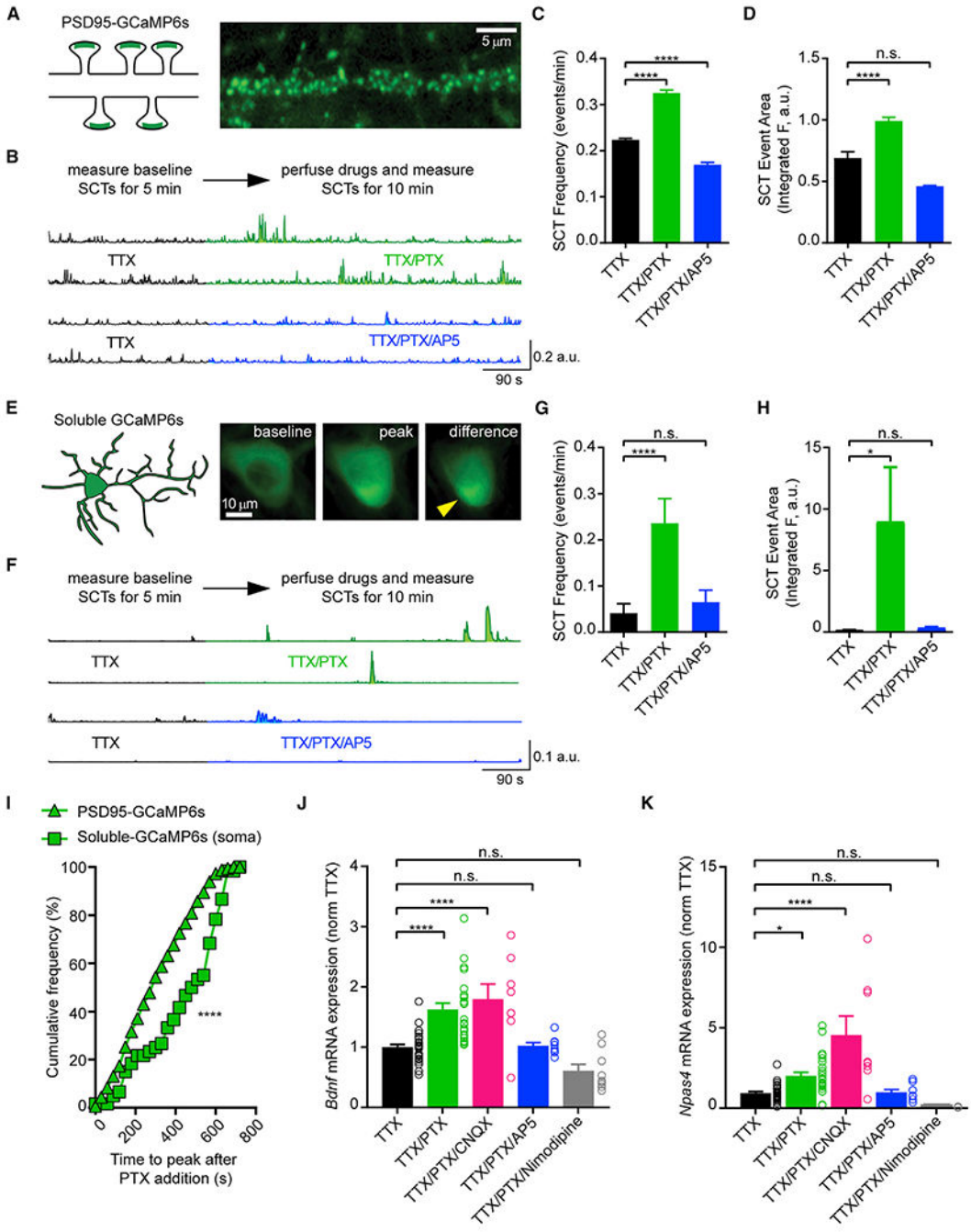

Figure 3. mIPSC block increases calcium signaling at excitatory synapses, leading to increases in *Bdnf* and *Npas4* mRNA

(A) Schematic and example image of PSD95-tagged GCaMP6s fluorescence.

(B) Representative traces (C and D). SCTs measured at synapses from same region of interest (ROI) 5 min before and 10 min after drug addition.

(C and D) Blocking mIPSCs with 1 µM TTX and 50 µM PTX increases the frequency (C, TTX, n = 8,050; TTX/PTX, n = 5,019; TTX/PTX/APV, n = 3,031; n is ROI) and area (D, TTX, n = 9,067; TTX/PTX n = 14,618, TTX/PTX/APV n = 3,046, n is events) of SCTs at excitatory synapses, but 50 µM AP5 abolishes this increase.

(E) Schematic and example image of soluble GCaMP6s fluorescence at soma.
(F) Representative traces (G–H). SCTs measured at somas from same ROI 5 min before and 10 min after drug addition.
(G and H) Blocking mIPSCs with 1 μM TTX and 50 μM PTX increases the frequency (G, TTX, n = 24; TTX/PTX, n = 24; TTX/PTX/APV, n = 33; n is ROI) and area (H, TTX, n = 4; TTX/PTX, n = 59; TTX/PTX/APV, n = 20, n is events) of SCTs at somas, but 50 μM AP5 abolishes this increase.
(I) SCTs increase at excitatory synapses before soma following mIPSCs block (PSD-95, n = 4,814; soma, n = 60; n is ROI).
(J and K) RNA was collected from cultured hippocampal neurons 6 h after drug treatment. Blocking AMPARs at rest with 10μM CNQX does not alter increased transcription of *Bdnf* (J, TTX, n = 27; TTX/PTX, n = 26; TTX/PTX/CNQX, n = 8; TTX/PTX/APV, n = 8; TTX/PTX/nimodipine, n = 9) and *Npas4* (K, TTX, n = 26; TTX/PTX, n = 26; TTX/PTX/CNQX, n = 8; TTX/PTX/APV, n = 8; TTX/PTX/nimodipine, n = 9). Blocking either NMDARs or L-type VGCCs at rest with 50 μM AP5 or 5 μM nimodipine, respectively, blocks increased transcription of *Bdnf* (J) and *Npas4* (K). Bar graphs are mean + SEM. Open circles next to bars = biological replicates. Experimental replicates unresolvable for imaging data. n.s., non-significant, *$p < 0.05$, ****$p < 0.0001$.
See also Figure S3 and Table S1.

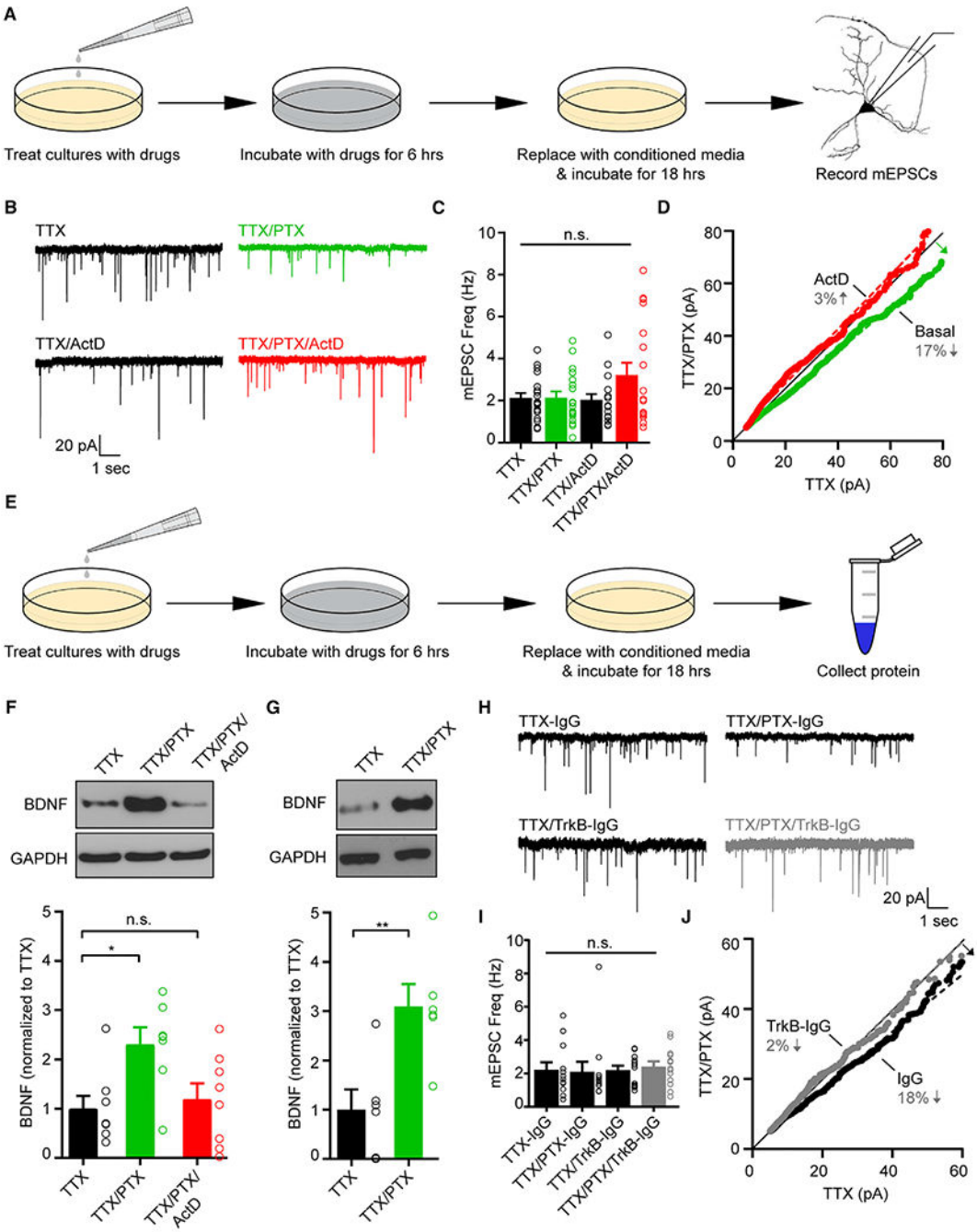

Figure 4. mIPSC block increases translation of newly transcribed *Bdnf* mRNA and leads to downscaling of mEPSC amplitudes

(A) Experimental schematic (B–D and H–J). mEPSCs recorded from cultured hippocampal neurons 24 h after initial 6 h drug treatment followed by a replacement of media with conditioned media for 18 h. ActD experiments: cells treated with ActD during initial 6 h drug treatment. TrkB-IgG experiments: cells treated with TrkB-IgG BDNF scavenger during 18 h incubation.

(B) Representative traces (C and D).

(C) mEPSC frequency is unaffected by drug treatment with 1 μM TTX, 50 μM PTX, and/or 2.5 μM ActD (TTX, n = 19; TTX/PTX, n = 18; TTX/ActD, n = 16; TTX/PTX/ActD, n = 18).

(D) Rank order plot of mEPSC event amplitudes. Initial blockade of mIPSCs downscales mEPSC amplitudes (basal, linear fit: $y = 0.8344x + 0.8319$, $R^2 = 0.9981$). Downscaling is abolished with 2.5 μM ActD treatment (ActD, linear fit: $y = 1.031x + 1.284$, $R^2 = 0.9870$).

(E) Experimental schematic (F and G). Protein was collected from cultured hippocampal neurons 24 h after initial 6 h drug treatment followed by a replacement of media with conditioned media for 18 h.

(F) Top: representative western blot. Bottom: BDNF is increased following initial block of mIPSCs with 1 μM TTX and 50 μM PTX. Increase is abolished with 2.5 μM ActD treatment (TTX, n = 8; TTX/PTX, n = 7; TTX/PTX/ActD, n = 8).

(G) Top: representative western blot. Bottom: BDNF is increased following initial block of mIPSCs with 1 μM TTX and 50 μM PTX if activity is blocked for experiment duration with 1 μM TTX (n = 6).

(H) Representative traces (I and J).

(I) mEPSC frequency is unaffected by treatment with 1 μM TTX, 50 μM PTX, 12.5 μg/mL IgG control, and/or 12.5 μg/mL TrkB-IgG (TTX/IgG, n = 12; TTX/PTX/IgG, n = 12; TTX/TrkB-IgG, n = 12; TTX/PTX/TrkB-IgG, n = 13).

(J) Rank order plot of mEPSC event amplitudes. Downscaling is abolished when BDNF is scavenged (IgG, linear fit: $y = 0.8159x + 0.8695$, $R^2 = 0.9963$; TrkB-IgG, linear fit: $y = 0.9783x + 0.5251$, $R^2 = 0.9934$). Bar graphs are mean + SEM. Open circles next to bars = biological replicates. Solid black line in (D) and (J) is unity line. n.s., non-significant, *p < 0.05, **p < 0.01.

See also Figure S4 and Table S1.

KEY RESOURCES TABLE

REAGENT or RESOURCE	SOURCE	IDENTIFIER
Antibodies		
Anti-GAPDH (Rabbit monoclonal)	Cell Signaling	Catalog # 14C10; RRID:AB_561053
Anti-BDNF (Rabbit monoclonal)	AbCam	Catalog # 108319; RRID: AB_10862052
Anti-ERK (Rabbit monoclonal)	Cell Signaling	Catalog # 4695S; RRID: AB_390779
Anti-pERK (Rabbit monoclonal)	Cell Signaling	Catalog # 4370S; RRID: AB_2315112
Anti-CREB (Rabbit monoclonal)	Cell Signaling	Catalog # 9197S; RRID: AB_331277
Anti-pCREB (Rabbit polyclonal)	Millipore	Catalog # 06-519; RRID: AB_310153
Chemicals, peptides, and recombinant proteins		
Picrotoxin	Sigma Aldrich	Catalog #P1675
Bicuculline	Sigma Aldrich	Catalog# 14340
D(−)-2-Amino-5-phosphonopentanoic acid (AP5)	AbCam	Catalog # A8054
Tetrodotoxin	Enzo Life Sciences	Catalog # BML-NA120-0001
CX614	Tocris	Catalog # 5149
Nimodipine	Tocris	Catalog # 0600
Ryanodine	Tocris	Catalog # 1329
Muscimol	Tocris	Catalog # 0289
Actinomycin D	Sigma Aldrich	Catalog # A1410
TTA-A2	AbCam	Catalog # ab145559
Recombinant Human IgG1 Fc, CF	R&D Systems	Catalog # 110HG100
Recombinant Human TrkB Fc Chimera Protein, CF (BDNF scavenger)	R&D Systems	Catalog # 688-TK-100
1,2,3,4-Tetrahydro-6-nitro-2,3-dioxo-benzo[f] quinoxaline-7-sulfonamide disodium salt hydrate (NBQX)	AbCam	Catalog # ab120046
QX314	EMD-Millipore	Catalog # E2692
DNase I	Sigma Aldrich	Catalog # D5025
Transferrin	Calbiochem	Catalog # 616420
Cytosine Arabinoside (ARAC)	Sigma Aldrich	Catalog # C6645
B-27 supplement	GIBCO	Catalog # 17504-010
FuGENE6	Promega	Catalog # E2692
Matrigel	Corning	Catalog # 354230
Critical commercial assays		
PureLink® RNA mini kit	Thermo Fisher Scientific	Catalog # 12183018A
PureLink® DNase set	Thermo Fisher Scientific	Catalog # 12185010
SuperScript® III Reverse Transcriptase kit	Thermo Fisher Scientific	Catalog # 18080085
PowerUp® *SYBR*® Green PCR Master Mix	Thermo Fisher Scientific	Catalog # A25777
Deposited data		
Raw and processed sequencing data	This paper	SRA: PRJNA734956
Experimental models: organisms/strains		

REAGENT or RESOURCE	SOURCE	IDENTIFIER
Sprague-Dawley rat pups (P1–P3)	Charles River	Strain code: 400
Oligonucleotides		
Primer: *Gapdh* Forward: AGGT CGGTGTGAACGGATTTG	This paper	N/A
Primer: *Gapdh* Reverse: TGTAGA CCATGTAGTTGAGGTCA	This paper	N/A
Primer: *Npas4* Forward: TATGGACTGCTACACCCCGA	This paper	N/A
Primer: *Npas4* Reverse: TAGCACAGCTGGGGTTCCTA	This paper	N/A
Primer: *Bdnf* Forward: AGACATGTTTGCGGCATCCAG	This paper	N/A
Primer: *Bdnf* Reverse: CCATAAGGACGCGGACTTGTACA	This paper	N/A
Primer: *Cfos* Forward: CAGAGCGGGAATGGTGAAGA	This paper	N/A
Primer: *Cfos* Reverse: TCGGTGGGCTGCCAAAATAA	This paper	N/A
Primer: *Arc* Forward: AGTAGGCACCAAACCCAAGG	This paper	N/A
Primer: *Arc* Reverse: AGCTATGCTGCCCAAGACTG	This paper	N/A
Recombinant DNA		
Plasmid: pRSV-REV (lentiviral packaging)	Dull et al., 1998	Addgene # 12253
Plasmid: pCMV-VSV-G (lentiviral packaging)	Stewart et al., 2003	Addgene # 8454
Plasmid: pMDLg/pRRE (lentiviral packaging)	Dull et al., 1998	Addgene # 12251
Plasmid: FUGW	Lois et al., 2002	Addgene # 14883
Plasmid: pGP-CMV-GCaMP6s	Chen et al., 2013	Addgene # 40753
Plasmid: FUGW-GCaMP6s	This paper	N/A
Plasmid: FUGW-GCaMP6f-PSD95	Reese and Kavalali, 2016	N/A
Plasmid: FUGW-GCaMP6s-PSD95	This paper	N/A
Software and algorithms		
MiniAnalysis	Synaptosoft	http://www.synaptosoft.com/MiniAnalysis
Clampfit	Molecular Devices	https://www.moleculardevices.com
Axopatch	Molecular Devices	https://www.moleculardevices.com
Prism 8	Graphpad	https://www.graphpad.com:443/
Fiji	Schindelin et al., 2012	N/A
MATLAB. (2018). 9.7.0.1190202 (R2019b).	Natick, Massachusetts: The MathWorks Inc.	https://www.mathworks.com/products/matlab.html?s_tid=hp_products_matlab